AIAA 97-2333 15th AIAA Applied Aerodynamics Conference

Transfer Function Analysis of Roll Moment Response to Stagnation Point Actuation

Darden, L.A.* and Komerath, N.M.†
School of Aerospace Engineering

Georgia Institute of Technology
Atlanta, Georgia 30332-0150

ABSTRACT

The Stagnation Point Actuator (SPA) has been shown to be an effective controller of forebody vortex asymmetry, roll moment, and wing rock at high angle of attack. This paper shows that the roll moment response to SPA deflection can be described by a set of linear transfer functions, which are classified into "families" of behavior based upon model attitude. From time series data of the roll moment and the SPA position, empirical transfer functions are calculated for 297 test conditions covering various sting angles, bank angles, tunnel speeds, and SPA actuation waveforms. The dependence of the frequency-averaged magnitude and the steady-state phase of each transfer function on angle of attack, bank angle, freestream speed, and actuation rate is studied. The roll moment transfer function magnitude appears to be independent of frequency in the range studied. Freestream speed is seen to have minimal effect, because the time scales of the roll and pressure response far exceed convection lags. This permits development of transfer function classes which depend primarily on angle of attack, with sub-classes based on bank angle.

NOMENCLATURE

C_l: Rolling moment coefficient
C_p: Difference in pressure coefficient across forebody based on freestream dynamic pressure. Positive for suction to the right.
f: frequency in cycles per second (Hz.)
H: frequency-domain transfer function
SPA: Stagnation Point Actuator
U_∞: Tunnel freestream velocity
ε: SPA deflection, deg., positive to the right
ϕ: Roll angle
σ: Sting (roll axis) angle relative to U_∞
γ^2: frequency-domain coherence function
S_{AA}: autospectral density distribution for input signal (SPA location in this case)
S_{BB}: autospectral density distribution for output signal
S_{AB}: cross spectrum between input and output signals.

INTRODUCTION

The stagnation point actuator (SPA) enables continuous, static and high-rate control of forebody vortex asymmetry. In previous papers[1,2,3], several features of this technique were shown. The device is successful in producing and suppressing forebody vortex asymmetry[1], inducing desired rolling moments on the wing-body[2], and in inducing and stopping large-amplitude wing rock[3]. These results provide strong evidence that effective control can be achieved under conditions where the aerodynamics are clearly nonlinear.

As is well-known[4], forebody vortices are seen when the angle of attack exceeds the half-angle of the forebody, and become asymmetric when the angle of attack generally exceeds twice that value. Forebody or noseboom strakes[5], or surface blowing at various locations and orientations on the forebody[6] have been used to force symmetry of the vortices after they are formed. Ref. 7 has proposed a scheme where the blowing is pulsed at a high repetition rate, with the duty cycle determining the degree of time-averaged yawing moment experienced by the aircraft.

The above techniques seek to control the vortices after they are formed. The Stagnation Point Actuator shown in Fig. 1 in contrast, triggers varying degrees of asymmetry at the very origin of the shear layers which roll up into the forebody vortices: the stagnation point at the nosetip. By displacing the stagnation point from the plane of lateral symmetry, the boundary layer development in the stagnation point flowfield is biased. To explore the effects of the SPA, we use a nose cone which can be yawed using a push-rod connected to a servo motor. The nose cone has the basic advantage of constant and simple surface geometry. Other versions of the SPA are easily imagined, where surface motion at the nosetip, or

---

* Graduate Fellow. Student Member, AIAA.
† Professor. Associate Fellow, AIAA.

blowing/suction serve to displace the stagnation point. Recently, Roos[8] has described effects of blowing at the front of a blunt nosetip.

Wing Rock Control

Forebody vortex asymmetry induces rolling moment on a winged body. The roll moment response is by no means simple. Our experiments[2,3] showed that the magnitude of the roll moment coefficients was as large as those induced by any of the other successful demonstrations of forebody vortex control and wing rock control[9]. In addition, we were able to introduce desired waveforms and rates of vortex asymmetry, and then observe the development of the effects downstream. Several competing processes with diverse time scales were observed. In free-to-roll tests, we found that wing rock could be induced and stopped very quickly by moving the SPA. This is shown in Fig. 2, from Ref. 9. The wing-body model was free to roll on a sting held at $\sigma = 40°$. In Fig. 2a, at 65 fps, the model goes into wing rock oscillations when the SPA is deflected 10° to the right, but the oscillations damp out. When flow speed is increased to 75 fps, the wing rock is pronounced and sustained (aerodynamic forcing has increased but the inertia remains the same) until the SPA is deflected back to the left, which stops the wing rock immediately. This showed that wing rock was induced and controlled by coupling between the forebody vortices and the wing flowfield. Even at the substantial yaw angle induced by the large-amplitude wing rock oscillation, the rolling moment induced by SPA motion was powerful enough to stop the rolling of the 4-lb model with steel wings instantly.

We have measured the rolling moment, as well as point measurements of the lateral pressure difference across the forebody at 3 sting angles and 11 bank angles, at 3 freestream speeds, in 2 different tunnels, using the same wing-body model [2,3]. In each case, the SPA was moved through several cycles of square-wave and sine-wave motion at 3 different frequencies. The data from these experiments thus consists of simultaneous, digitized records of roll moment, pressure difference and nose deflection angle. We have shown that linear relations exist between any two of these three measured quantities at a given test condition. These results are represented as transfer function values at 128 different frequencies. Several interesting phenomena are seen in these results. This paper takes a large step towards a full physical description of roll moment behavior: it shows that the roll moment behavior can be classified into a few regimes. Inside each regime, only a few parameters are important, and the behavior is quite linear.

Objectives

In this paper, we report the results of efforts to reduce the complexity of describing the roll response. It will be shown that the system transfer functions can be grouped into families of behavior, valid over specific regimes of model attitude. The steady state phase and the frequency averaged magnitude of the transfer function are used to describe the behavior. The parameters of interest are σ, ϕ, U_∞, actuation rate, and the effects of wind tunnel wall proximity. Our data show that the vast majority of wind tunnel measurements reported in the literature to date on this problem are likely affected by the tunnel walls.

DETAILS OF THE EXPERIMENTS

The model used in the experiments[1,2,3] (Fig. 4) is a delta wing/body of revolution with equal root chord and span (Aspect Ratio of 2.0) and has a cylindrical fuselage with 50.8 mm outer diameter. The AR2Δ wing is a flat steel plate with sharp edges beveled at 18° on the lower surface. Its geometric sweep of 63.47° puts it between the 60°and 65° wings chosen for extensive study elsewhere. The body-of-revolution nose ends in a conical nose tip with a semi-apex angle of 15° and a length of 0.03 m. A servo motor in the fuselage rotates the nose in the yaw plane under computer control. We verified that servo actuation induces no rolling moment on the model in still air. The nose tip deflects through the yaw range $-10° < \varepsilon < 10°$. Maximum lateral deflection of the nose tip stagnation point is 8.1 mm.

In each of the experiments, the model is sting-mounted with a steel rod along the roll axis. A moment balance attached to the sting uses flexures and strain gages to measure the instantaneous rolling moment of the model. The first group of experiments was performed in the 1.07m x 1.07m (42" x 42") AeroControls Wind Tunnel at the School of Aerospace Engineering. The model was rigidly mounted to the moment balance at zero yaw and bank angles and tested at σ = 20°, 30°, 35°, 40°, and 45°. Data at 45, 50, 55, 60 and 65 ft/s were obtained at each σ. The roll moment response to square wave excitation of the nose tip was examined. Excitation frequencies of 0.1, 0.5, and 1.0 Hz were used, and roll moment data were taken for periods and sampling rates as outlined in Table 1, reproduced from Ref. 2.

Table 1: Sampling Parameters for the Square Wave Nose Deflections

Wave Frequency	Sampling Rate	Sampling Time
1.0 Hz	100 Hz	20 seconds
0.5 Hz	100 Hz	30 seconds
0.1 Hz	100 Hz	60 seconds

The second set of experiments were performed in the 2.1 m x 2.74 m John J. Harper Wind Tunnel. The tunnel cross-section area is 4.56 times that of the AeroControls tunnel. The same model is used in the two windtunnels. For these experiments, roll moment is measured at σ = 35°, 40°, and 45° for U_∞ of 55, 65, and 75 fps. Furthermore, the effect of finite ϕ on roll moment response to SPA deflection was explored. Bank angle was varied over the range $-5° < \phi < 5°$ in 1° steps. Square wave SPA deflections at 0.1, 0.5 and 1.0 Hz were used, and roll moment data were taken as outlined in Table 2, from Ref. 3.

Table 2: Sampling Parameters for Square Wave Nose Deflection Tests

Wave Frequency	Sample Rate	Sample Time
1.0 Hz	50 Hz	15 seconds
0.5 Hz	50 Hz	20 seconds
0.1 Hz	50 Hz	30 seconds

Measurement Uncertainty

The strain gage balance allowed no more than 0.25° roll at the highest moments measured in this paper. The uncertainty in moment measurement was 5%. The frequency response of the strain gage sensor/conditioner was flat beyond the range of interest.

DATA REDUCTION

Simultaneous time series of nose position, rolling moment and lateral pressure difference, were obtained during each of the 297 test conditions outlined. Each data set contained samples obtained at 750 to 6000 time steps, the time between steps being fixed at 0.01 or 0.02 seconds. The nose and moment data were read as time series A and B respectively. Auto spectra were used to verify the frequency range of the data. The signals were then re-sampled with specified sampling rates, slower than the original 100 or 50 Hz, to limit the frequency range and use the available number of frequency intervals to improve the frequency resolution. The sampling parameters are given in Table 3. A random number generator was used to start each sample block at a random point in the data set, and 1000 such samples were used in the ensemble averaging of the results: this removed any phase bias.

Table 3: Sampling Parameters in Data Reduction

Nose Oscillation Frequency	Number of Points Skipped	Frequency Increment
0.1 hz	20	.02 hz
0.5 hz	10	.06 hz
1.0 hz	5	.08 hz

Each sample block was transformed to the frequency domain using a Fast Fourier Transform algorithm. The analysis procedure is one that has been used widely in the digital signal processing community, as well as in structural dynamics, acoustics, and turbulent combustion, and follows the standard treatment given in Ref. 10. The reasons to use such procedures are detailed in Appendix A.

The autospectral density distributions ("autospectra") of A and B were obtained as $S_{AA}(f)$ and $S_{BB}(f)$. The cross spectrum between A and B, a complex function of frequency, was obtained as $S_{AB}(f)$. The coherence between A and B is then

$$\gamma^2(f) = |S_{AB}|^2 / (S_{AA} * S_{BB})$$

The criterion for linearity is the proximity of the coherence to the value 1.0 at the frequency of interest. At frequencies where the coherence is high (in this paper we rejected all data where the coherence was lower than 0.8), the transfer function values are considered to be reliable. The transfer function is the complex function

$$H(f) = S_{AB} / S_{AA}$$

This function is essentially the ratio between B and A, broken down by frequency. The magnitude at each frequency is the "sensitivity" of B to A, and the phase is the phase between B and A at that frequency. Thus, for example, a dead time lag such as a convection lag would show up as a straight line phase variation, since the same time interval would represent increasing portions of the cycle at higher frequencies.

Because the input signals (the nose motion) were either sine waves (1 frequency) or square waves (fundamental plus odd harmonics), most of the fluctuation energy of the input signals is contained within a few frequencies. The linearity of the relationship between the two signals A and B (which is verified by the coherence being close to unity) guarantees that what happens at one frequency does not affect what happens at another. We cannot calculate the transfer function at frequencies where the coherence is low: at these frequencies, the input signal may not have much energy, or there may be uncorrelated noise present. Nonlinear effects (the relationship varying with the amplitude of the signals) may also contribute to this "noise". The selected data points of high coherence are then used to represent the transfer function in a compact form, as was shown to be feasible in Ref. 9. Given that 80 to 90 percent of the signal fluctuation energy is captured by these points, it is acceptable to interpolate through these frequencies to find transfer function values at intermediate frequencies. Obviously, the more coherent data points available in a data series, the greater the confidence one has in this procedure,

but the only error source is if the poor coherence at intermediate points is due to some unexpected nonlinear phenomenon. Only 27 of the 297 test cases contained fewer than 4 highly coherent data points.

RESULTS

Except where noted otherwise, all of the data presented below were obtained in the larger John J. Harper wind tunnel. These are assumed to be free of tunnel wall effects, the test section area being 4.56 times larger than the 1.07m x 1.07m tunnel where the data of Ref. 2 were obtained. The blockage in the 1.07m tunnel is less than that reported in the literature for most high angle of attack forebody asymmetry experiments[3].

Piecewise Linear Transfer Function description

Despite the apparent complexity of these phenomena, several encouraging observations have been made. The transfer functions measured from the experimental data are obtained with 128 frequency channels each, so that a series of 128 complex numbers are needed to represent it in a Fourier series. However, Fig. 3 from Ref. 9 shows that a linear transfer function, represented by a few terms of the Fourier series, represents the roll moment response to SPA deflection quite well (excellent coherence), in roll-constrained experiments for a given test condition. Excellent coherence is obtained over the frequency range of the square-wave signal's frequency content.

SPA Rate Effects Negligible

The magnitude of the transfer function is approximately constant over the range where coherence is high. In addition, we verified that transfer function magnitudes at the higher frequencies, obtained from the 0.1Hz SPA square wave data, matched the values at those frequencies computed from 0.5 and 1Hz SPA square wave data. This shows that the rate of SPA deflection does not change the response in this range of rates. The matching of transfer function magnitudes from runs with different SPA square wave frequencies is especially encouraging: it confirms that there are no buried nonlinearities. This major simplification enables us to use the Average Magnitude of the transfer function, over the frequency range of interest, to represent the "sensitivity" of the roll moment to SPA deflection for the purposes of summarizing the roll moment behavior.

Phase Variation with Frequency

The phase of the transfer function shown in Fig. 3 is interesting. It is monotonic, and indicates time scales much longer than the simplistic model of freestream convection lag. The monotonic nature relieves our concern (stated above) about mysterious nonlinear phenomena being buried in the frequency intervals where coherence was low. Had there been any such surprises, one would expect to see discontinuities or at least inflexion points in the phase variation.

Steady-State Phase

The value of the phase at steady state (the limit as frequency tends to zero) is interesting. If the roll moment had the same sign as the SPA motion, this phase would be zero. If the moment has the opposite sign from the SPA deflection, the phase would be 180 ° If processes of both signs compete, something in between would result. Again, we use the steady-state phase in this paper to summarize the roll-moment behavior, noting that the phase variation with frequency is indeed significant, and needs further flow experiments to understand.

Influence of σ and ϕ on Steady State Phase

For this discussion, we ask the reader to look at both Figs. 5 and 6. Fig. 5 illustrates our hypotheses, and presents simultaneous time traces, at $\phi = 0°$, of the SPA deflection angle, the lateral pressure coefficient difference across the forebody at a station close to the nosetip, and the roll moment coefficient based on span (which is equal to the root chord for the AR2Δ wing). Fig. 6 illustrates the behavior of the steady state phase of the SPA - roll moment system at σ = 35, 40, and 45 ° We see that each angle of attack regime has its own phase signature, with bank angle influencing the system at $\sigma = 35$ and 40°

The $\sigma = 45°$ case (see Figs. 5a and 6) shows a consistent zero degree phase over the entire range of bank angles tested. This means that positive SPA deflection (to the right from a pilot's viewpoint) creates a positive roll moment (right wing down). As Fig. 5a shows, we do not expect interaction between the forebody vortices and the wing vortices at this angle of attack. In Ref. 3 we hypothesized that at $\sigma = 45°$ the mechanism by which the roll moment is created is dominated by the creation of a pressure difference across the forebody of the model. This pressure difference induces a small cross-flow component of velocity which increases the effective angle of attack on the left wing. The result is a greater lift on that wing, and hence a roll moment. Since no evidence of forebody vortex interaction with the wing leading edge vortices has been observed at this test condition, one would not expect that banking the symmetric forebody would create any variation in the roll moment response. The data of Fig. 6 is consistent with this hypothesis. The roll moment (Fig. 5a) is small, but is monotonic, as compared to what happens in Figs. 5 b and c.

Let us now skip for a moment to Fig. 5c. The mechanism by which roll moment is created at

σ = 35° is quite different[3]. In this case, the forebody vortices propagate back to the wing, interacting with the leading edge vortices. This strengthens the vortex over the wing toward which the actuator has been deflected, increasing that wing's lift. The result is a quick-acting roll moment in the opposite direction of SPA deflection (SPA to the right creates right wing up moment). Fig. 6 displays the expected 180 ° phase shift for bank angles greater than or equal to -1°. However, for bank angles of -3 and -4 ° the steady state phase is 90 ° and for -5 ° bank the phase is 130°. This raises new questions which are not completely understood at present. One might expect that banking the aircraft to large angles could create a situation in which the forebody vortex on the side of the upward tilted wing continues to interact with that leading edge vortex, while the vortices on the other side of the body are positioned too far apart for interaction. This would result in a type of hybrid situation in which roll moment is created by two battling mechanisms. Such a situation could explain the phase behavior seen in Fig. 6 over the negative bank angles, but provides no explanation for the phase behavior seen at the positive bank angles. The reason for the asymmetric behavior with bank angle remains unclear at this time.

Figure 5c shows another phenomenon. Note that the moment response to the first and third nose deflections looks greatly different from the response to the second one. This is a repeatable phenomenon: we have several traces showing the same kinds of events. This suggests a phenomenon with a time scale of 15 to 20 seconds in a flow experiment where the freestream speed is 65 fps! The most probable culprit is the long-time-scale movement of the vortex bursting locations, reported in Refs. 11 and 12. This remains a mystery pending flow visualization experiments. Given that the vortex burst plays a part in this regime, we may attribute one of the two competing shorter time-scale events above to other aspects of the wing vortex response. Again this requires further experiments on basic fluid mechanics.

The σ = 40° case represents a complex interaction of roll moment creation mechanisms. It is believed that at 40° incidence, roll moment is created by some partial interaction of forebody vortices and wing leading edge vortices with the pressure mechanism seen at higher angles of attack still providing some influence[3]. One would then expect to see some combination of phase angles from the 35° and 45° cases playing a role in the 40° transfer function. However, one would not expect the results of Fig. 6, in which these conflicting phases are grouped into families of behavior based on bank angle. Considering the zero phase seen at bank angles less than or equal to -1°, it would seem the pressure differential mechanism dominates in this range of attitudes, while the vortex interaction mechanism creates the 180 ° phase behavior seen at positive roll attitudes. Once again the reason for the asymmetric behavior with bank angle remains undetermined at this time. Lacking other explanations, we blame the popular bogeyman, "Vortex Bursting", and suggest that the vortex bursting on the two wings may be triggered at slightly different effective angles of attack.

An explanation of the omission of several data points in Fig. 6 is in order. At σ = 40°, the data points for ϕ = 3 and 5° were omitted as a result of measurement uncertainty. Basically, there were too few coherent data points at these test conditions to determine the steady state phase with any certainty. The data points at (σ = 35°, ϕ = ± 2°) and at (σ= 40°, ϕ = +2°) have also been omitted, but for other reasons. All of the data points included in Fig. 6 are consistent for U_∞ = 55, 65, and 75 ft/s. The three omitted data points have steady state phase values which vary with speed. More will be said on this subject later.

Influence of σ and ϕ on Average Magnitude

Fig. 7 illustrates the behavior of the transfer function frequency averaged magnitude with bank angle at the three sting angles tested. The average magnitude of the transfer function is influenced by σ and ϕ. Notice that over the entire range of bank angles tested, the average magnitude is greatest at 35 ° angle of attack and least at 45 ° angle of attack. This is consistent with our discussion on roll moment creation mechanisms found in the previous section. The vortex interaction mechanism is much stronger than the induced flow mechanism and should be expected to create greater roll moments.

At σ = 45 °, the magnitude is essentially independent of ϕ except for a slight increase at negative ϕ. At σ = 35°, the peak occurs at ϕ =+1°. The values at positive ϕ are substantially higher than those at negative ϕ: this asymmetry was seen in the phase values of Fig. 6, and may be due to the vortex bursting sensivitity alluded to there. The σ = 40° case also peaks at ϕ = + 1° . Close examination reveals that this plot again has slightly higher values at positive ϕ. However, the variation in magnitude is compressed such that one could approximate the behavior as a scattering about the mean of 0.0003.

The asymmetric behavior of the transfer function magnitude and the occurrence of the maximum magnitudes at non-symmetric attitude remains unexplained at present. However, the variation with ϕ is much less than the variation with σ, so that the primary variable is clearly the angle of attack.

Effects of U_∞ on Transfer Function Properties

It is interesting to note that freestream speed has almost no effect on the transfer function

properties of the SPA - roll moment coefficient system. At each sting angle and bank angle, nine test cases were run: square wave SPA deflections at 0.1, 0.5, and 1.0 Hz each at 55, 65, and 75 ft/s. In comparing the transfer function average magnitude at each of the related nine test cases, it was found that the variation in magnitude at different speed conditions was random and well within the variation found between different SPA deflection rate conditions for each given speed. Furthermore, the variation in average magnitude found between different actuation rate tests was also random and insignificant. For these reasons, the data points plotted in Figs. 6 and 7 were obtained by averaging the values of steady state phase and mean magnitude for each of the nine combinations of SPA deflection rate and freestream speed tested at each angle of attack and bank angle.

In comparing the steady state phase values obtained for different actuator rates and freestream speeds, it was found that these two properties had absolutely no effect on steady state phase for all but three model attitudes. The exceptions are interesting to note. At (σ = 35 °, ϕ = -2 °), the steady state phase varies both in actuation rate and freestream speed but with no discernible pattern. At (σ = 35 °, ϕ = +2 °), there exists a drop in steady state phase from 180 ° at 55 and 65 ft/s to only 90 ° for 75 ft/s. Similarly, at (σ = 40 ° , ϕ = +2°), there is a drop in steady state phase from 180 ° at 55 and 65 ft/s to 0° for 75 ft/s. The reason for these anomalies is as yet undetermined; it suggests that one or other of the competing processes changes with U_∞ in this range, possibly due to Reynolds number dependence.

Wall Effects on Transfer Function Properties

The transfer function results for the model mounted at ϕ = 0° in two windtunnels differing in wall interference by a factor of 4.56 were compared. It was found that the proximity of the wall introduced significant differences in steady state phase, the average magnitude variation with angle of attack, and the effect of freestream speed on the transfer function properties.

The wall effect on steady state phase introduces some interesting issues. To begin, the proximity of the wall has no effect on steady state phase at σ = 40° and 45°; under both test conditions the steady state phase at σ = 40° is 180° and at σ= 45 ° is 0°. However, when the model is mounted at σ = 35° , the wall effects will introduce a 180 ° shift in the steady state phase of the SPA - roll moment transfer function. The steady state phase in the absence of wall effects is 180°, while under the influence of wall effects the phase is 0° . This represents a transformation in the system behavior from a situation dominated by interaction between forebody and wing leading edge vortices to a behavior that resembles the pressure differential -based roll moment mechanism seen earlier for higher angles of attack. This would seem to indicate that the effect of the upper wall's proximity to the upper surface of the model is to mitigate those vortex interactions.

Table 4a: Comparison of Transfer Function Average Magnitude With and Without Wall Effects at 55 ft/s Freestream Speed

Sting Angle σ	42" tunnel	7' x 9' tunnel
35°	.0014	.0013
40°	.0052	.00051
45°	.049	.00014

Table 4b: Comparison of Transfer Function Average Magnitude With and Without Wall Effects at 65 ft/s Freestream Speed

Sting Angle σ	42" tunnel	7' x 9' tunnel
35°	.0015	.0023
40°	.0049	.00059
45°	.082	.000098

The data of Table 4 display the interesting effect that wall proximity has on the transfer function average magnitude. Notice that in the absence of wall effects average magnitude increases with decreasing σ. Yet with wall effects present, the opposite effect holds; average magnitude decreases with decreasing sting angle. If the hypothesis proposed from the observations on steady state phase are true and the result of the wall's close proximity is indeed to mitigate the vortex interactions, then these data are consistent with the roll moment magnitude behavior expected. If the only mechanism available to create roll moment on the model is the induced angle of attack variation created through the forebody pressure differential, it makes sense that the model would experience greater variations in wing lift at greater angles of attack.

We have already discussed the very minor effect that freestream speed has on the transfer function properties in the absence of wall effects. When testing the model in the smaller wind tunnel, we again notice only very minor variations in transfer function properties as a result of freestream speed variations. Indeed, at σ = 35 and 40°, there is no noticeable variation with speed in either steady state phase or transfer function average magnitude. At σ = 45°, the only noticeable speed effect is a slight increase in average magnitude with increasing speed.

CONCLUSIONS

1. The complex roll moment response to SPA deflection can be described by a set of simple linear transfer functions.

2. Transfer function magnitude appears to be constant over the range of frequencies tested, and are repeatable between runs made with different SPA square wave frequencies.

3. The transfer functions describing the system's behavior at various test conditions can be classified into "families" of behavior.

4. The transfer functions are insensitive to freestream speed, except for phase variations at certain bank angles.

5. The most influential factor in classifying the system transfer function is the model's angle of attack. Three distinct classes of steady state phase and average magnitude performance were observed.

6. At high angles of attack, the forebody vortices appear to have little effect on the wing vortices, and the roll response appears to be due to changes in effective angle of attack.

7. At moderate angle of attack, wing vortex response dominates the roll response to SPA deflection.

8. At intermediate angles of attack, competing and opposite processes are observed in the roll response.

9. A long time scale response is observed at moderate angle of atttack, and attributed without direct evidence to vortex bursting.

10. Within each main transfer function class, sub-classes based upon the system response variation with bank angle have been identified. Surprisingly, the sub-classes are not symmetric with bank angle.

11. The proximity of the wind tunnel walls to the model have been shown to substantially change the transfer function behavior.

These results show that over small bank angles, the roll response of a wing-body to SPA deflections (forebody vortex perturbation) can be described in a simple, piecewise linear manner with a few well-behaved parameters.

ACKNOWLEDGMENTS

This work was performed under AFOSR AASERT Grant F49620-93-1-0342, monitored by Maj. Daniel Fant and Dr. Len Sakell. The first author received support from an NSF Graduate Fellowship. Assistance from other members of the Experimental Aerodynamics research team is gratefully acknowledged.

REFERENCES

1. Darden, L.A. and Komerath, N.M., "Forebody Vortex Control at High Incidence Using a Moveable Nose Stagnation Point", AIAA 95-1775, 13th Applied Aerodynamics Conference, June '95.
2. Darden, L.A., Peterson, K.G., and Komerath, N.M., "Vortex Control Using a Moveable Nose with Pressure Feedback", AIAA 95-3468, Atmospheric Flight Mechanics Conference, August '95.
3. Peterson, K.G., Darden, L.A., and Komerath, N.M., "Dynamic Roll Control Experiments Using a Moveable Nosetip", AIAA 96-0789, 34th Aerospace Sciences Meeting, January '96.
4. Ericsson, L.E. and Reding, J.P., "Asymmetric Vortex Shedding from Bodies of Revolution", Tactical Missile Aerodynamics, Vol. 104, 243-296.
5. Murri, D.G., Shah, G.H., DiCarlo, D.J., and Trilling, T.W., "Actuated Forebody Strake Controls for the F-18 High-Alpha Research Vehicle", Journal of Aircraft, Vol. 32, No. 3, May-June, '95.
6. Celik, Z.Z., Pedreiro, N., and Roberts, L., "Dynamic Roll and Yaw Control by Tangential Forebody Blowing", AIAA-94-1853, June '94.
7. Lee, R., Hanff, E., Kind, R., "Wind Tunnel Investigation of Dynamic Manipulation of Forebody Vortices". AIAA 95-1794, June '95.
8. Roos, F., "Microblowing for Vortex Asymmetry Management on a Hemisphere-Cylinder Forebody". AIAA 96-1951, June '96.
9. Darden, L.A., Peterson, K.G., and Komerath, N.M., "Roll Control Using a Stagnation Point Actuator", AIAA 96-2498, 14th Applied Aerodynamics Conference, June '96.
10. Bendat, J. S. and Piersol, A. G., Random Data Analysis and Measurement Procedures, 2nd edition, John Wiley and Sons, New York, 1986.
11. Pamadi, B.N., Rao, D.M., Niranjana, T., "Wing Rock and Roll Attractor of Delta Wings at High Angles of Attack", AIAA 94-0807, Jan. '94.
12. Jenkins, J., "Nonlinear Aerodynamic Characteristics of a 65 Degree Delta Wing in Rolling Motion: Implications to Testing and Flight Mechanics Analysis", AIAA 97-0742, Jan. '97.

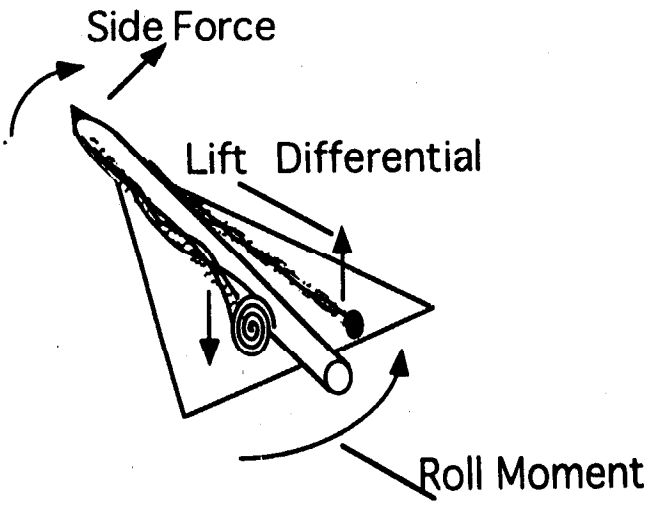

Figure 1: Schematic of Forebody Vortex Induced Forces and Moments on the Delta-Wing Model with SPA(Ref. 9)

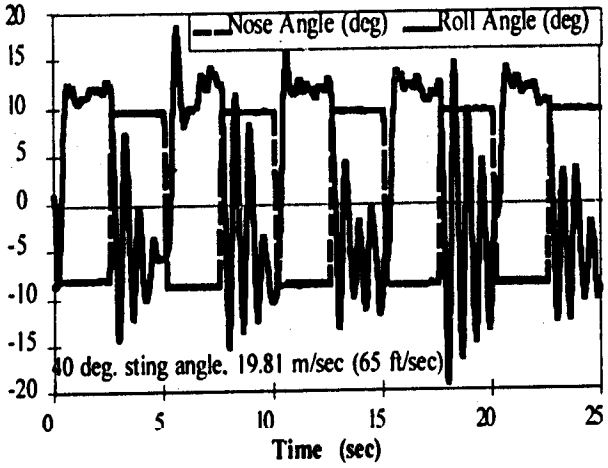

Figure 2a: Free-to-Roll Time History at 40 deg. sting angle and 19.81 m/s (Ref. 9).

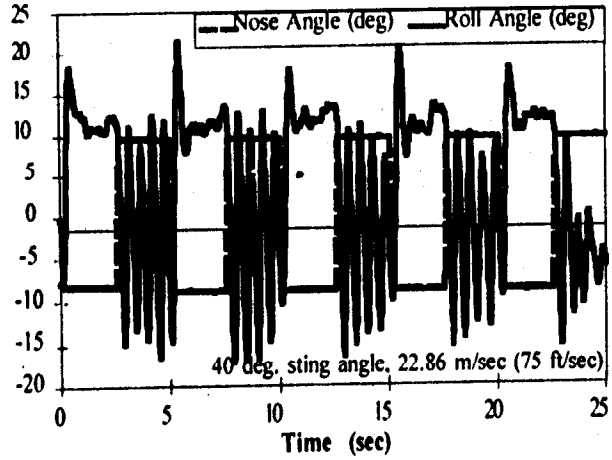

Figure 2b: Free-to-Roll Time History at 40 deg. sting angle and 22.86 m/s (Ref. 9)

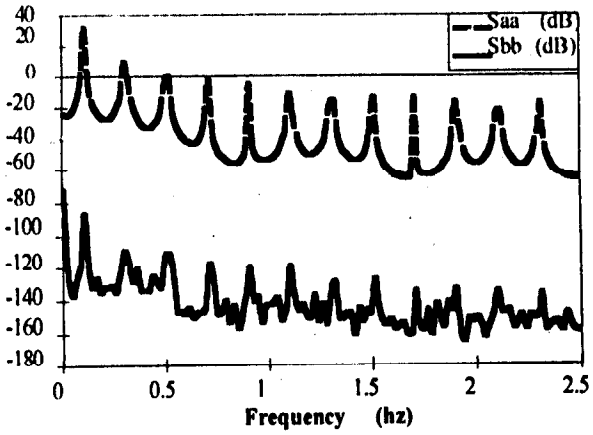

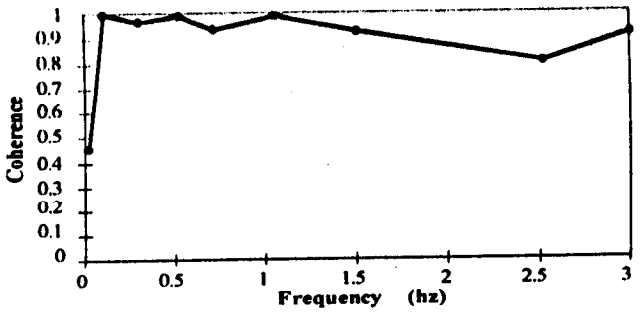

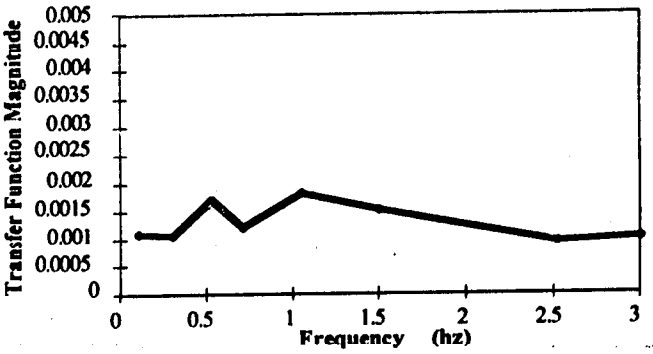

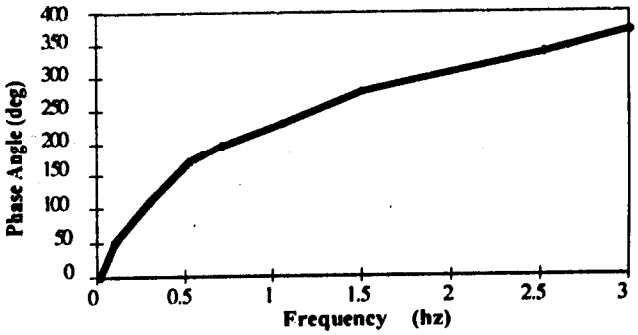

Figure 3: Autospectra and Transfer Function Coherence, Magnitude, and Phase of SPA - Roll Moment Coefficient System at 35 deg. sting angle, 45 ft/s, 0 deg. bank, and 0.1 Hz SPA rate tested in AeroControls Tunnel (Ref. 9)

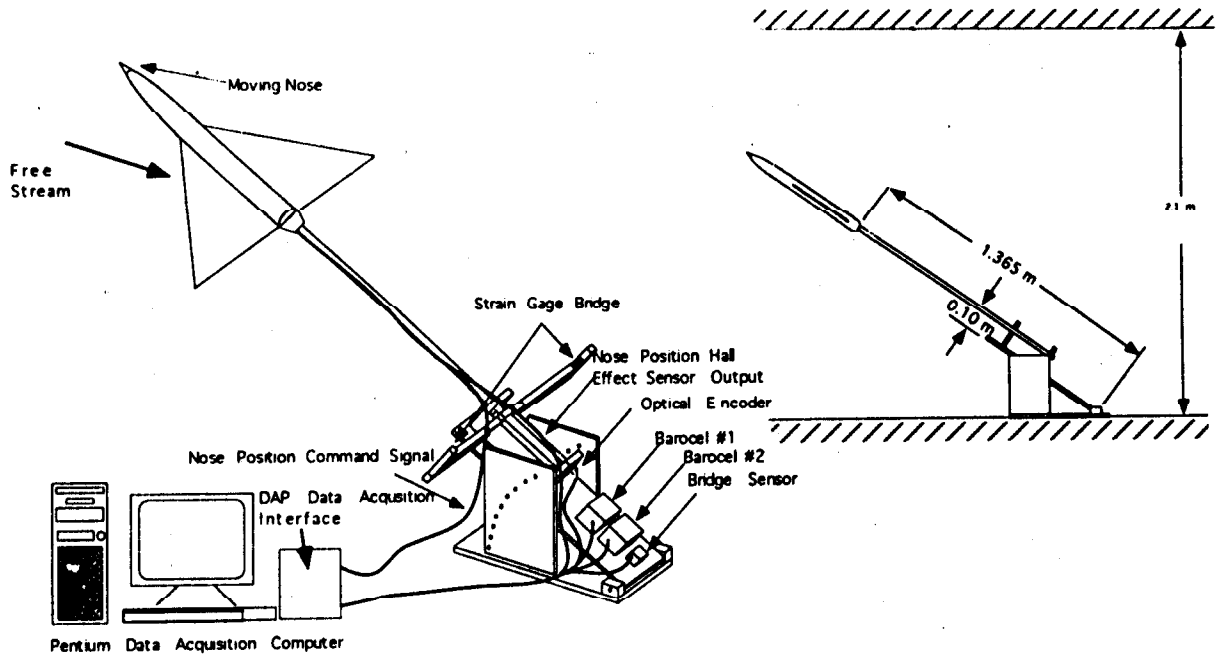

Figure 4a: AR2D Wing-Body Model on Roll Balance

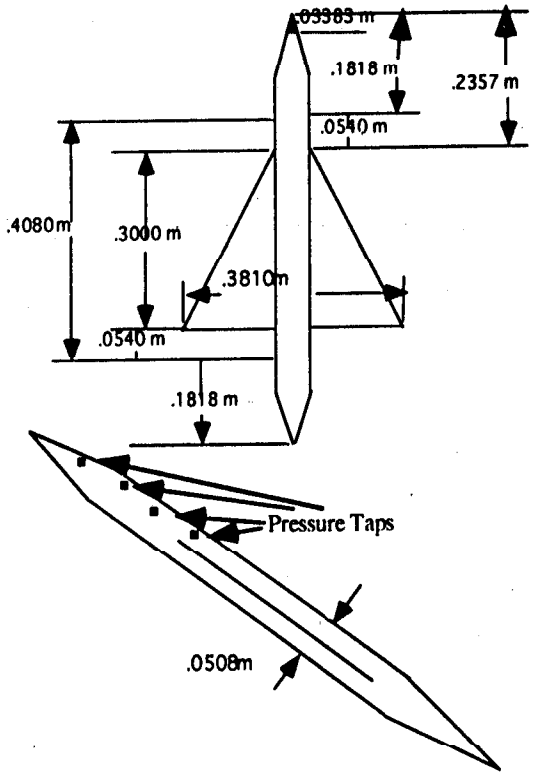

Figure 4b: AR2D Wing-Body Model with Location of Static Pressure Taps Indicated

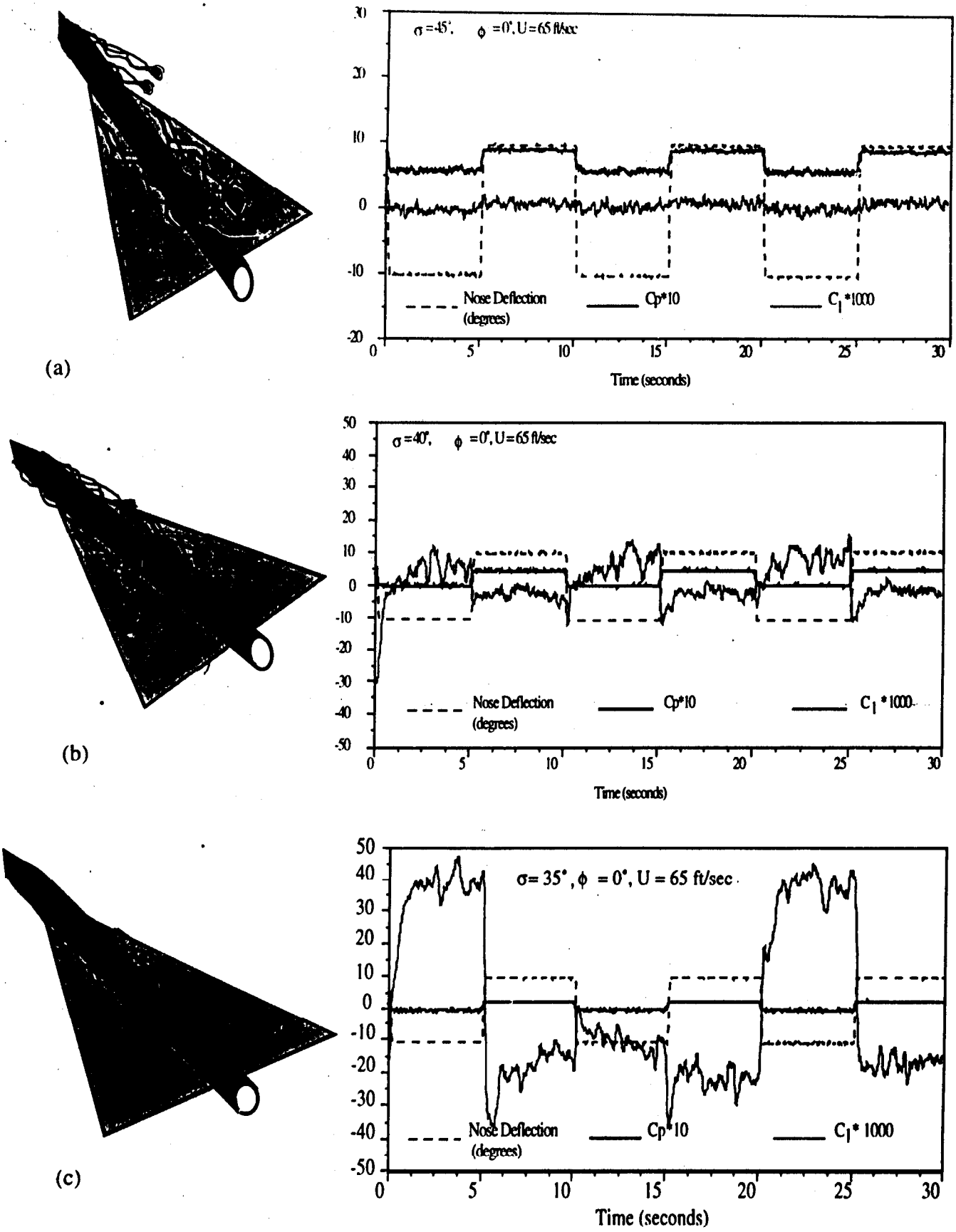

Fig. 5: Angle-of-attack dependence of roll moment response to SPA deflection. Rolling moment coefficient and SPA deflection are plotted as functions of time. (a) High angle of attack behavior. (b) Intermediate angle of attack, with vortex bursting over the wings. (c) Moderate angle of attack with maximum vortex interaction.

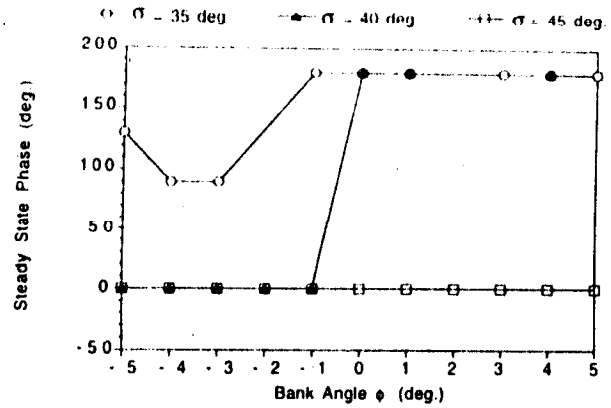

Fig. 6: Steady state phase of the SPA - roll moment system for various sting angles as a function of bank angle, averaged over speed

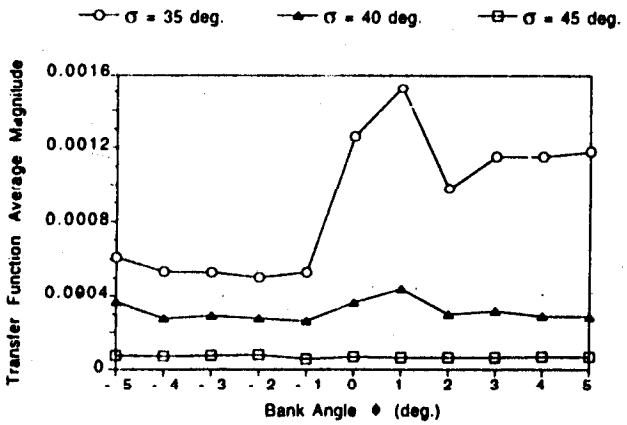

Fig. 7: Transfer function frequency-averaged magnitude of the SPA - roll moment system for various sting angles as a function of bank angle, averaged over speed

APPENDIX A

Transfer Functions for Aerodynamics

The use of transfer functions in the context of a High Angle of Attack Aerodynamics paper has excited some questions of relevance from experts in this community, which we seek to answer in the following. The authors thank readers for their patience. To describe the aerodynamic behavior of aircraft under the conditions described above, and to do so in a manner useful to the development of control systems, we must venture outside the steady-state data acquisition and interpretation techniques traditionally seen in the Applied Aerodynamics literature on high angle-of-attack aerodynamics. For example, if one were to plot the instantaneous roll moment against the instantaneous SPA position, the result would be a meaningless scattergram. In the past, such mundane problems appear to have obscured the fact that there is a linear causal relationship between the forebody vortex asymmetry and the wing rolling moment. In fact forebody asymmetry was believed by some to be a chaotic phenomenon. More recently, researchers have begun to include the convective time lag in their data interpretation. However, a surprising result encountered in the forebody vortex problem is that we observe several time scales, some of which are upto 2 orders of magnitude longer than the convective time lag. Similar lags have been reported in the roll response of isolated delta wings (Ref. 12) and a wing-body (Ref. 11). To capture such phenomena, one requires carefully designed data acquisition and analysis schemes. For example, consider that the sampling duration has to be long enough to capture fluctuations with a period 100 times as long as the convection lag. In water tunnels, where the flow velocities are on the order of a few millimeters per second, this would lead to sampling times so long that freestream velocity cannot be held constant over such times. In low-speed wind tunnels of moderate size, the time resolution of the data has to be short enough to capture convection times of a few milliseconds. The process of budgeting analog-digital converter channels, tunnel time and computer disc space would normally dictate sampling times that are much shorter than those required to capture these phenomena.

As a first step towards developing an aerodynamic description amenable to control system development, we have shown that the wing rolling moment obeys piecewise linear transfer functions, which can be represented in compact form. These transfer functions are simply expressions of the ratio of the dependent variable (rolling moment, for example), to the independent variable (SPA position, or aileron angle), as functions of the frequency (rate) of the variation in the independent variable. The transfer function value in each frequency interval is a complex number, the phase being needed to express the temporal relationship between the independent and dependent variables.

The extraction of such transfer functions assumes that there is a linear, causal relationship between the independent and dependent variables. This implies the satisfaction of two criteria: first, of the existence of a cause-effect relationship, and second, of the relationship being independent of the amplitude of the variables at any of the frequencies (rates) under consideration. Obviously, discontinuous and multiple-valued functions would pose problems: such problems are expected in the analysis of wing rolling moment at high angles of attack. The coherence function between the independent and dependent variables measures the validity of these assumptions. Values near unity, in the range of frequencies where there is substantial energy content in the input, provide confidence that a linear, causal relationship exists, thus justifying the use of the transfer function approach.